frontiers

Supplementary Material

1 Supplementary Information

1.1 Neoproterozoic Stratigraphy of Northeastern Svalbard

The Neoproterozoic strata of northeastern Svalbard are part of the Hecla Hoek Series, which span from the middle Proterozoic to the early Paleozoic in age. The distribution of Neoproterozoic rocks in this region is shown in **Figure S1**. These rocks were deformed during the Scandian phase of the Caledonian orogeny, and again during latest Cretaceous to early Cenozoic opening of the North Atlantic Ocean. They nevertheless remain very well preserved in terms of both textures and geochemistry, making them ideally suited to studying Neoproterozoic Earth history. Additional information on the distribution of outcrops and on the stratigraphy can be found in Halverson et al. (2007a) and Halverson et al. (2018a).

1.2 Correlated ages used in the age-height model

Ten radioisotopic dates from other sedimentary basins are incorporated into this model (**Table 1**). These are a combination of Re-Os dates on organic-rich sediments and U-Pb zircon CA-ID-TIMS dates, mostly on felsic tuffs. The individual radioisotopic dates and the basis for the correlation with the Svalbard Tonian reference section are provided below, organized by region. Note that the uncertainties shown in **Table 1** and incorporated in the model include the full uncertainty related to the isotopic tracers and decay constant so as to be able to compare between different isotopic systems (i.e. U-Pb and Re-Os). As a consequence, the uncertainties shown here may not be identical to those in the text of the original sources for these dates. The height uncertainties are assigned either a normal distribution (where the correlation is guided by salient $\delta^{13}C_{carb}$ trends) or a uniform distribution (where the $\delta^{13}C_{carb}$ trends are less distinctive). The uncertainties shown in Table 1 correspond either to the 95% range for normal distributions or the full range for uniform distributions.

1.2.1 Northwestern Canada

Proterozoic inliers containing well exposed and complete Neoproterozoic successions occur in Yukon and western Northwest Territory. Multiple radiometric dates—both Re-Os and U-Pb zircon ages—have been obtained from these strata (**Figure 3**), including the first dates used to refine the age of onset of Cryogenian glaciation to ca. 717 Ma (Macdonald et al., 2010). A tuff bed (F834–147.5) in the lower Fifteenmile Group (Reefal Assemblage) in the Coal Creek inlier is dated at 811.41±0.45 Ma sits about 100 m below the onset of a negative $\delta^{13}C_{carb}$ anomaly interpreted to be the Bitter Springs Anomaly (BSA) and above a peak in $\delta^{13}C_{carb}$ (Macdonald et al., 2010). We correlate this tuff to 430 m in the Svalbard reference section, 32 m below the onset of declining $\delta^{13}C_{carb}$ leading into the BSA (**Figure 2**). A similar Re-Os date of 810.7 ± 6.13 Ma has been obtained from just below the inferred onset of the BSA in Fifteenmile Group of the Tatonduk inlier near the border with Alaska (Cohen et al., 2017). We place this age at 450 m in our reference section, 12 m below the start of the decline. Due to their stratigraphic association with the BSA, both ages are assigned relatively low stratigraphic uncertainty (80 and 40 m, respectively).

The Little Dal Group is a thick succession of middle–late Tonian platformal carbonates in the Mackenzie Mountains that correlates with the Fifteenmile Group and similarly preserves the BSA (Halverson, 2006; Macdonald et al., 2010). Locally, the Little Dal Group is capped by the Little Dal basalt, which comprises up to nine mafic flows with a maximum thickness of 92 m (Jefferson and Parrish, 1989). The Little Dal basalt is associated with the Tsezotene sills in northwestern Canada and considered to be an extrusive product of the ca. 779 Gunbarrel Large Igneous Event, which includes dykes as far south as Wyoming (Harlan et al., 1993). A more precise age of the Little Dal basalt has recently been established through a U-Pb zircon CA-IDTIMS date of 775.1±1.0 Ma on diabase dyke crosscutting the basalt (Milton et al., 2017). Aitken (1981) interpreted the contact between the uppermost Little Dal Group, the Ram Head Formation (formerly the "upper Carbonate"), to be conformable. Our observations at upper Boomerang Lake in the northern Mackenzie Mountains confirm the conformable contact, indicating that this date provides a tight age constraint on the uppermost Little Dal Group. **Figure S2** presents a stratigraphic log and $\delta^{13}C_{carb}$ profile through the upper Ram Head Formation at this locality and a comparison to a complete $\delta^{13}C_{carb}$ profile through the Little Dal Group at Coppercap Mountain, further south in the Mackenzie Mountains (Halverson, 2006). In that section, the Cryogenian Sayunei Formation sits directly on the Ram Head Formation, such that both the Little Dal basalt and the Coates Lake Group, which post-dates the Little Dal basalt, are missing below the unconformity (**Figure S2**). Even deeper levels of erosion on this surface have been documented (Jefferson and Parrish, 1989). Both carbon isotope stratigraphy and sequence stratigraphy imply that the upper Ram Head Formation at Boomerang Lake is mostly if not entirely younger than the uppermost Ram Head Formation on Coppercap Mountain, consistent with the relatively small amount of strata that occur above the inferred BSA in the middle Ram Head Formation in that section. The Boomerang Lake section shows distinctive cyclicity in the $\delta^{13}C_{carb}$ record atop overall low $\delta^{13}C_{carb}$ values (by Tonian standards), which is also characteristic of the middle Backlundtoppen Formation in Svalbard (**Figure 2, Figure S2**). Therefore, we tentatively place the Little Dal basalt age in the middle Backlundtoppen Formation (1675 m) and ascribe a uniform uncertainty of 100 m.

The late Tonian Callison Lake Formation in Yukon is the equivalent of the Coates Lake Group in the Mackenzie Mountains, based on a combination of tectonostratigraphic considerations, chemostratigraphy, and geochronology (Strauss et al., 2014, 2015; Rooney et al., 2015). We correlate two Re-Os from the Callison Lake Formation to Svalbard using the tectonostratigraphic correlations proposed by Halverson et al. (2018a)(**Figure 2**). The older date of 752.7±5.5 Ma is from the lowermost Callison Lake Formation and corresponds to a recovery from low $\delta^{13}C_{carb}$ values; we ascribe this age to the middle Kinnvika Member in the uppermost Akademikerbreen Group (1960 m) with normal uncertainty (95%) of 40 m. A second age of 739.9±6.1 Ma occurs near the nadir of a deep negative carbon isotope anomaly in the upper Callison Lake Formation, which correlates with a similar anomaly in the Coppercap Formation of the Coates Lake Group and is also interpreted to correlate with the Russøya negative $\delta^{13}C_{carb}$ anomaly in Svalbard (Halverson et al., 2018a). It is assigned a height of 2097 m with an uncertainty of 40 m A third Re-Os age of 732.2±3.9 (Rooney et al., 2015) occurs in the middle Coppercap Formation, just above the crossover back to positive $\delta^{13}C_{carb}$ values in the recovery from the Russøya Member. This return to positive values is absent in Svalbard but is projected above the current top of the Russøya Member (2190 m) with a uniform uncertainty of 80 m, based on the assumption of a continuous trend towards positive values as seen in the Coppercap Formation.

1.2.2 Ethiopia

The well preserved, mixed carbonate-siliciclastic Tambien Group and of northeastern Ethiopia has yielded many high-precision U-Pb zircon dates that are central to calibration of the Tonian Period (Swanson-Hysell et al., 2015; MacLennan et al., 2018; Park et al., 2019)(**Figure 3**). The oldest direct age on the Tambien Group is on a tuff in the Werii Formation at the base of the group, with an age of 815.29±0.99 Ma (Swanson-Hysell et al., 2015). Although this age is from a shaley interval, it clearly lies beneath what is regarded as the Bitter Springs Anomaly, which occurs in the overlying Assem Formation. Swanson-Hysell et al. (2015) suggested a correlation with the penultimate peak in $^{13}C_{carb}$ prior to the onset of the BSA. Based on that correlation, we ascribe that age to a height of 250 m in the Svalbard reference section, with a uniform uncertainty of 150 m to account for the lack of tight carbon isotope control on its placement. Two younger ages of 788.72±0.94 Ma and 787.38±0.82 Ma have been obtained on tuffs of the upper Tsedia Formation (Swanson-Hysell et al., 2015). These ages provide a minimum age constraint on the end of the BSA, but due to limited structure in the carbon isotope record in this interval, it is hard to establish a robust correlation with the Svalbard reference section. Because both ages are close and overlapping, we use only one of the ages here (788.72 Ma), and we place this at a height of 1125 m, with a large uniform uncertainty in stratigraphic range of 200 m. Two older tuffs within the Tsaliet Group equivalent of the lower Tambien Group have been dated at ca. 796–794 Ma (Park et al., 2019), but because they are not associated with carbonate strata, they cannot be correlated with Svalbard.

Several younger ages have been obtained from latest Tonian strata in Ethiopia, and these provide excellent constraints on the onset of Cryogenian glaciation (MacLennan et al., 2018). Of relevance here is a date of 735.35±0.88 Ma obtained on a tuff in the lower Matheos Formation. This age corresponds to the recovery from the older of two negative $\delta^{13}C$ anomalies in the late Tonian (Halverson et al., 2019a), which we correlate with the Russøya anomaly in Svalbard. We project this age to 2175 m in the Svalbard reference section, which is just above the top of the present Russøya Member in the reference section but would capture the return towards positive values were it not erosionally truncated. We apply an uncertainty of 80 m.

1.2.3 Northern Namibia

Neoproterozoic strata are widespread in Namibia, but Tonian-aged strata are relatively less abundant and do not extend beyond about 770 Ma. While ca. 746 Ma volcanics have been dated in northern Namibia (Hoffman et al., 1996), the dated localities do not cooccur within carbonate strata, making them difficult to correlate with Svalbard. However, a U-Pb zircon (air abrasion TIMS) weighted Mean $^{207}Pb/^{206}Pb$ date of 759.95±0.86 on a tuff in the upper Devede Formation of the Ombombo Subgroup was reported by Halverson et al. (2005). We have updated this date in order to account for decay constant uncertainty, yielding a modified $^{207}Pb/^{206}Pb$ age of 759.9±2.4 Ma (**Figure S3**). The Devede Formation displays a quasi-cyclic trend towards higher $\delta^{13}C_{carb}$, reminiscent of the upper Backlundtoppen Formation. We correlate this date with 1850 m in the Svalbard reference section and apply a normal height uncertainty of 100 m.

1.3 Bayesian Subsidence Model

The code for our Bayesian subsidence model is written in the R programming language and formatted in Markdown mode. It can be downloaded from https://github.com/gphalverson/Svalbard-age-model-2021. The code is fully annotated within the R Markdown file.

This code requires four additional files to run. The first file ('height_age.csv') contains the age, height, and uncertainty data from Table 1 and a second contains the key heights for which model ages and 95% credibility intervals should be calculated ('plot_heights.csv'). A third file ('Svalbard_composite.csv') contains all of the carbon isotope data and corresponding heights in the composite reference section plotted in Figure 2. The code assigns an age and 95% maximum and minimum value for each of these heights so that all data can be plotted versus age. Similarly, the file 'Sr_composite.csv' contains heights for a compilation of strontium isotope data from the Akademikerbreen Group interpreted to represent primary seawater values (from Cox et al., 2016). All of these files, which should be placed in the same folder as the code, can also be found on the GitHub site.

The code utilizes functions from the "rethinking" package of McElreath (2020). The Bayesian model fit runs after each bootstrapping of original ages and heights. The model is currently set to run 5000 iterations.

The code generates several output .csv files which records the median ages and uncertainties: for key heights in the succession (i.e. Table 2), at 5 m intervals, for every height for which there is carbon isotope data, and for every height for which there are strontium isotope data. The 1D Uniform Stretching Thermal Subsidence Model

The simple thermal subsidence model used here (Figure S3) was originally derived and described by McKenzie (1978) and Steckler and Watts (1978). It has previously been applied to subsidence modelling of Neoproterozoic sedimentary basins (e.g. Halverson et al., 2002; LeGuerroué et al., 2006). The equation and its parameters are thoroughly described in Allen and Allen (2013). In summary, it calculates the subsidence resulting from cooling and densification of new, hot, mantle lithosphere following instantaneous stretching by a factor of β and as result of diffusional heat flow through the overlying crust. The result is a logarithmically decreasing rate of subsidence with time, as seen on passive continental margins.

The equation for sediment-loaded thermal subsidence as a function of time, S(t) can be simplified to

$$S(t) = E_0 \frac{\beta}{\pi} \sin\left(\frac{\beta}{\pi}\right)\left(1 - e^{\left(\frac{-t}{\tau}\right)}\right)$$

Where τ is the thermal time constant for the lithosphere and is defined as

$$\tau = \frac{y_L^2}{\pi^2 \kappa}$$

with y_L being the thickness of the lithosphere and κ its thermal diffusivity, and

$$E_0 = \frac{4y_L\rho_m^*\alpha_v T_m}{\pi^2(\rho_m^* - \rho_s)}$$

Here, ρ_m^* is the density of mantle at a temperature of 0ºC, ρ_s is the density of the sediment fill, α_v is the coefficient of thermal expansion, and T_m is the temperature at the base of the lithosphere. For sediment density, we make the simplifying assumption of early lithification of shallow water carbonates, which allows us to disregard sediment densification as a consequence of compaction (Halvereson et al., 2002). We also do not consider eustatic fluctuations in sea level because these are of short duration compared to the total duration of thermal subsidence.

For the purpose of this model, we have fixed the values of all of the parameters other than the stretching factor; these are listed below. We could, in theory, allow other parameters to vary as well, which could provide insight on the state of the Svalbard lithosphere, but doing so will not noticeably influence our age model because the different parameters would adjust to yield similar best-fit curves to the age-height data.

Parameters	**Value**	**Description**
y_L	125 km	Thickness of the lithosphere
ρ_m^*	3330 kg/m^3	Density of the mantle at 0ºC
ρ_s	2600 kg/m^3	Density of sediments
α_v	3.28x10^{-5} ºC^{-1}	Coefficient of thermal expansion
T_m	1333ºC	Temperature at base of lithosphere
κ	1x10^{-6} m^2/s	Thermal diffusivity of lithosphere

1.4 Smoothing fit to $\delta^{13}C_{carb}$ data

Figure 10 and **Table S2** present age-calibrated fits to a composite carbon isotope record spanning the Akademikerbreen and Russøya Member (lower Polarisbreen Group). All available data have been 'mapped' into the Svalbard Tonian reference section by correlating by individual members and adjusting heights as needed to compensate for variations between individual sections and the reference section (Halverson et al., 2018a). A customized, non-parametric LOESS-like smoothing algorithm was applied to this composite dataset in order to generate an evenly spaced and smoothed

mean value, along with 95% uncertainty intervals. This smoothing algorithm was run with 10 m windows (for 5-m resolution), with a least-squares regression fit to all data within each 10 m window. The mean value and uncertainties were calculated from the middle of each window (i.e. 5 m). We did not apply weighted means as in typical LOESS (locally weighted running line smoother) algorithms because our intention was to capture trends, although the difference between this method and a standard LOESS fit is nominal.

2 Supplementary Figures and Tables

2.1 Supplementary Figures

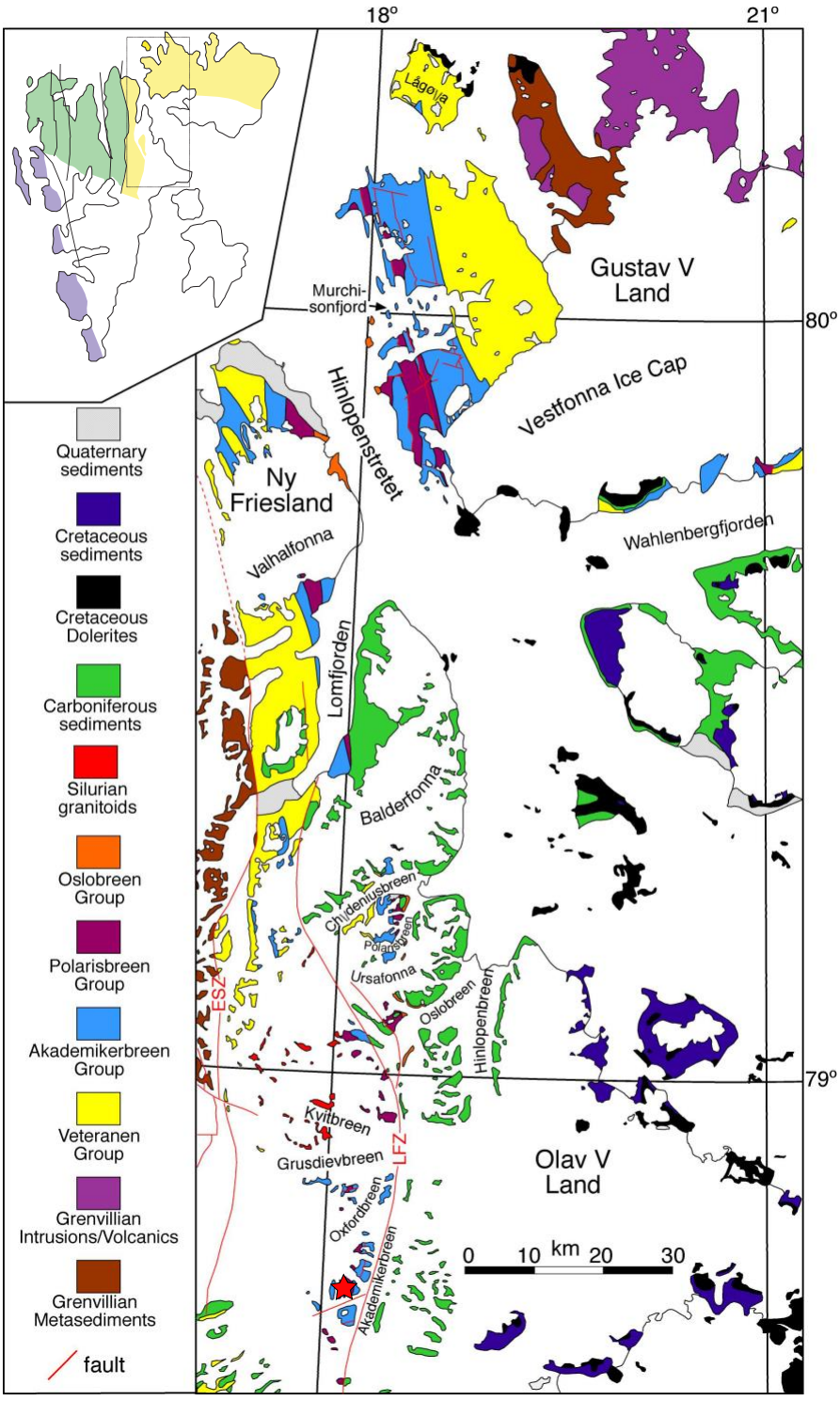

Supplementary Figure 1. Geological map of northeastern Svalbard showing the distribution of Neoproterozoic outcrop (Veteranen, Akademikerbreen, and Polarisbreen groups) in the study area.

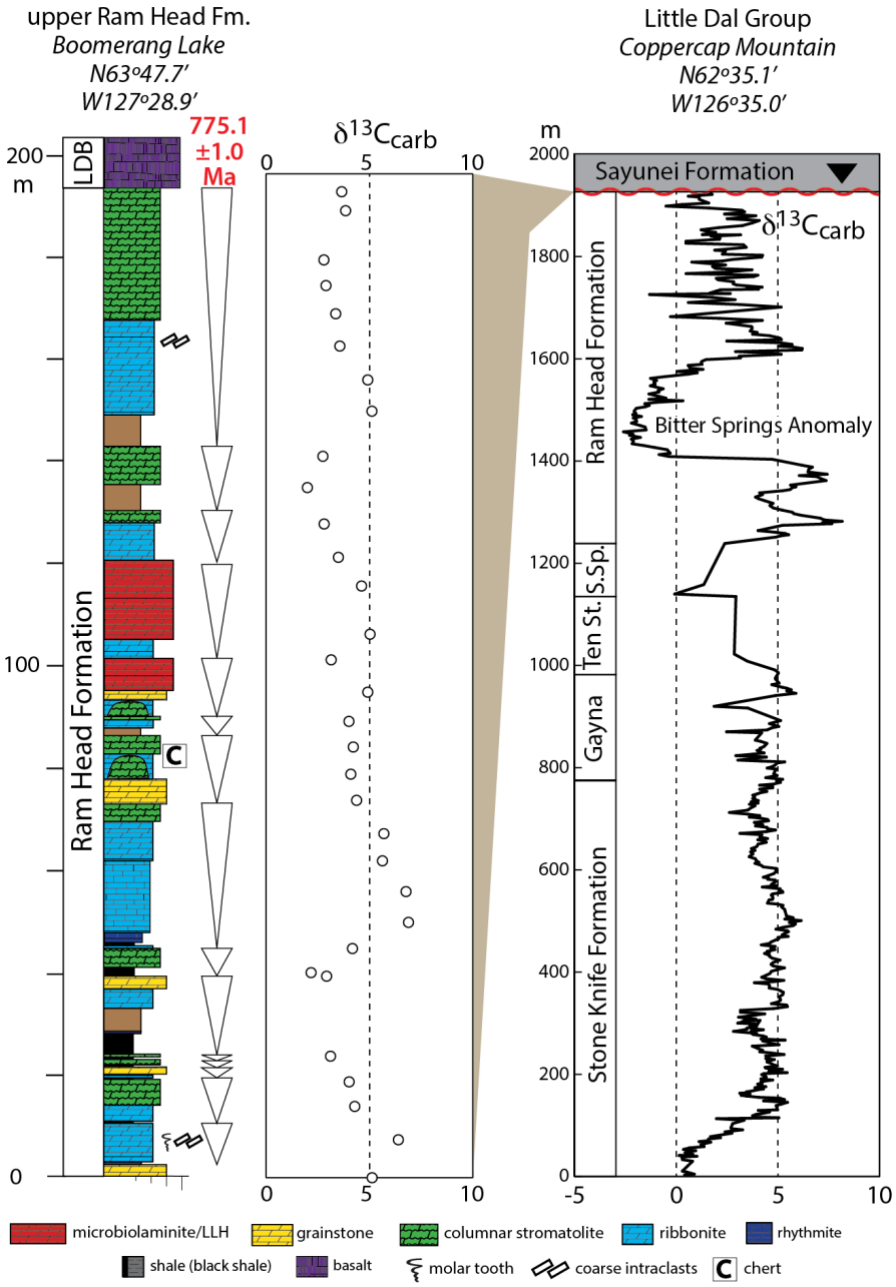

Supplementary Figure 2. Stratigraphic log of a section of the uppermost Little Dal Group (Ram Head Formation) at Boomerang Lake, northern Mackenzie Mountains (left), and its proposed correlation with the Little Dal Group reference section on Coppercap Mountain (Halverson, 2006). Note that no erosion is inferred between the Ram Head Formation and Little Dal Basalt at Boomerang Lake, whereas significant erosion beneath the Sayunai Formation (Rapitan Group) is evident in the Coppercap Mountain section, accounting for the fact that the entirely of the section measure at Boomerang Lake is believed to be missing at Coppercap Mountain. Data for the Boomerang Lake section is included in **Table S1**.

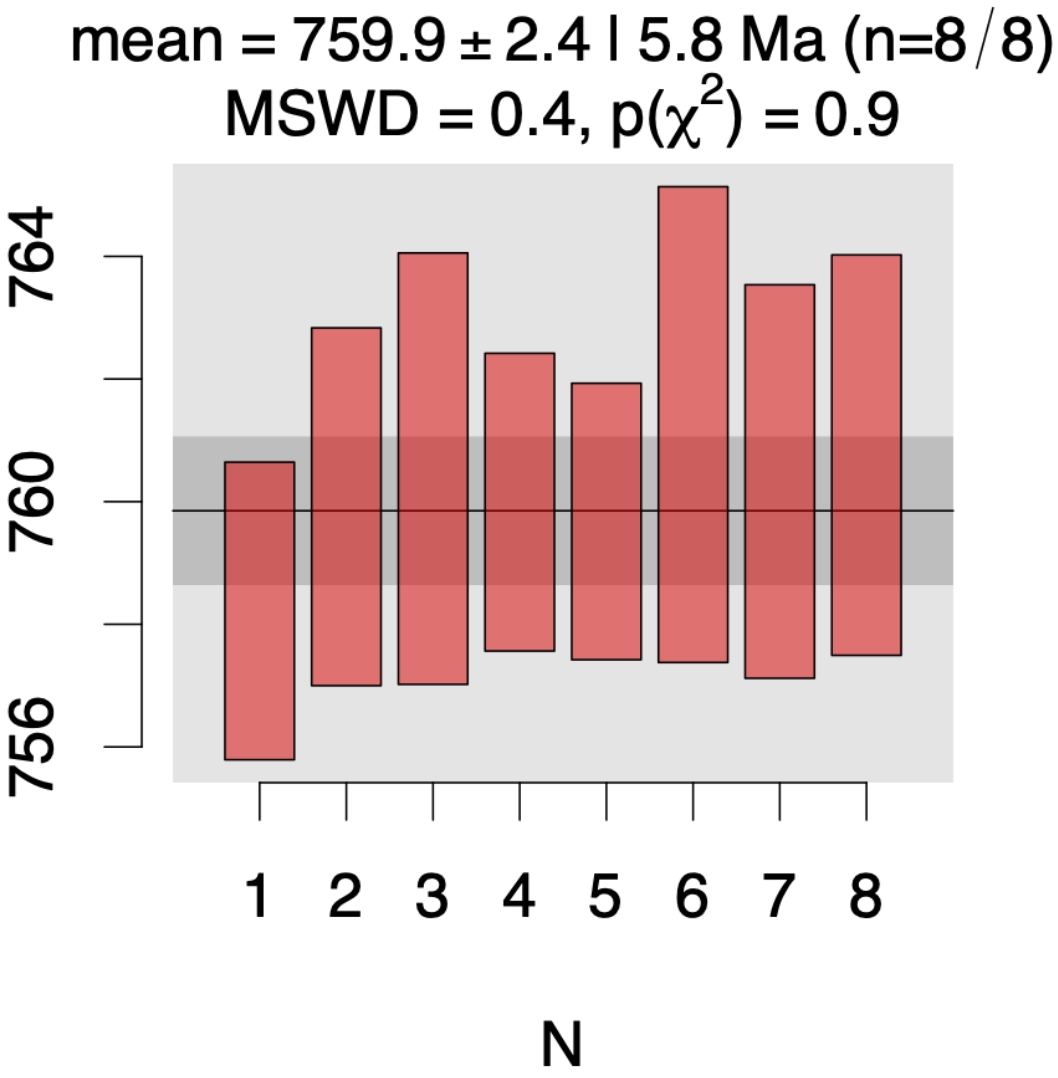

Supplementary Figure 3. Weighted mean $^{207}Pb/^{206}Pb$ date on a tuff in the upper Devede Formation of the Ombombo Subgroup in northern Namibia, based on data published in Halverson et al. (2005) and updated to incorporate decay constant uncertainty using IsoplotR (Versmeech et al., 2018).

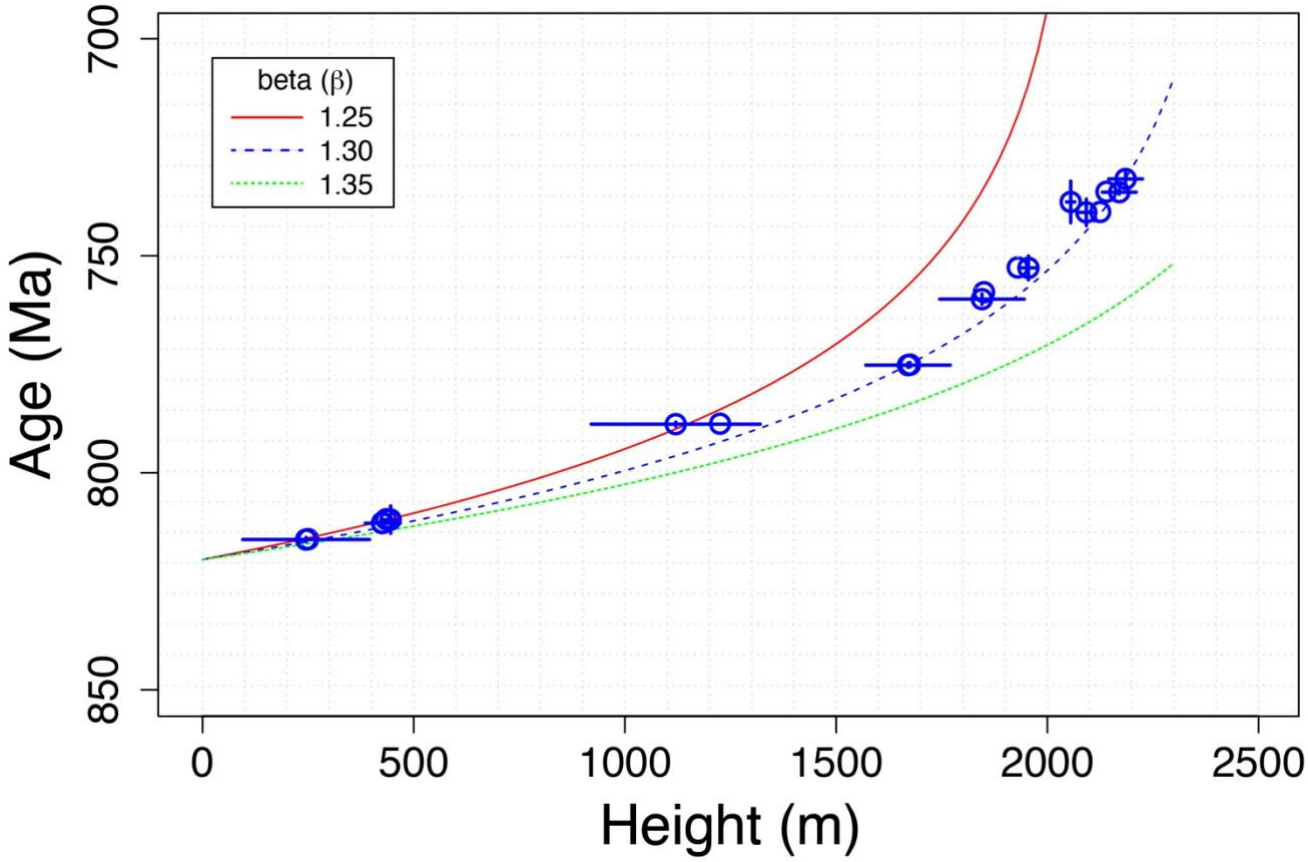

Figure S4. Ages, heights, and uncertainties of the dates correlated to the Svalbard Tonian reference section (**Table 1**), along with 1D uniform stretching thermal subsidence curves for stretching (β) factors of 1.25, 1.3, and 1.35. Visually, it is evident that β=1.30 is a better fit to the data, but a thorough analysis of this fit should include the uncertainties, which is easily accomplished through a Bayesian quadratic approximation approach.

2.2 Supplementary Tables

Supplementary Table 1. Carbon and oxygen isotope data (previously unpublished) from the Boomerang Lake section of the upper Ram Head Formation (G23; see also **Figure S2**). The data were acquired in the Laboratory for Chemical Oceanography at Harvard University following methods described in Halverson et al. (2007a).

Supplementary Table 2. Model output median ages and 95% credibility intervals at 5 m spacing for the Svalbard Tonian reference section, along with corresponding $\delta^{13}C_{carb}$ data and 95% uncertainties from our smoothing algorithm.

Supplementary Table 3. Compilation of all strontium isotope ($^{87}Sr/^{86}Sr$) data from the Akademikerbreen Group and Russøya Member in Svalbard inferred to record primary seawater compositions, along with corresponding ages from our age-height model. Data are from Halverson et al. (2007b) and Cox et al. (2016).

3 References

Aitkin, J. D., 1981. Stratigraphy and sedimentology of the Upper Proterozoic Little Dal Group, Mackenzie Mountains, Northwest Territories. In Campbell, F. H. A. (Ed.). Proterozoic Basins of Canada: Geological Survey Paper 81-10, pages 47–71. Geological Survey of Canada.

Allen, P.A. and Allen, J.R., 2013. Basin Analysis: Principles and Applications to Petroleum Play Assessment (3rd Edition). Wiley-Blackwell, 632 pp.

Cox, G. M., Halverson, G. P., Stevenson, R. K., Vokaty, M., Poirier, A., Kunzmann, M., Li, Z.-X., Denyszyn, S. W., Strauss, J. V., and Macdonald, F. A., 2016. Continental flood basalt weathering as a trigger for Neoproterozoic Snowball Earth. Earth and Planetary Science Letters 446, 89–99.

Halverson, G. P., 2006. A Neoproterozoic Chronology. In Xiao, S. and Kaufman, A., editors, *Neoproterozoic Geobiology and Paleobiology*, Topics in Geobiology Vol. 27, pages 231–271. Springer, Dordrecht, the Netherlands.

Halverson, G. P., Dudás, F. Ö., Maloof, A. C., and Bowring, S. A., 2007b. Evolution of the $^{87}Sr/^{86}Sr$ composition of Neoproterozoic seawater. Palaeogeography, Palaeoclimatology, Palaeoecology 256, 103–129.

Halverson, G.P, Hoffman, P.F., Kaufman, A.J., and Schrag, D.P., 2002. A major perturbation of the carbon cycle before the Ghaub glaciation (Neoproterozoic) in Namibia: prelude to snowball Earth? *Geochemistry, Geophysics, Geosystems* **3**, 10.1029/2001GC000244.

Halverson, G. P., Hoffman, P. F., Schrag, D. P., Maloof, A. C., Rice, A. H., 2005. Towards a Neoproterozoic composite carbon isotope record. Geological Society of America Bulletin 117, 1181–1207.

Halverson, G. P., Kunzmann, M., Strauss, J. V., Maloof, A. C., 2018a. The Tonian-Cryogenian transition in Svalbard. Precambrian Research 319, 79–95.

Halverson, G. P., Maloof, A. C., Schrag, D. P., Dudás, F. Ö., Hurtgen, M. T., 2007a. Stratigraphy and geochemistry of a ca 800 Ma negative carbon isotope interval in northeastern Svalbard. Chemical Geology 237, 5–27.

Harland, S. S., Heaman, L., LeCheminant, A. N., and Premo, W. R., 1993. Gunbarrel mafic magmatic event: A key 780 Ma time marker for Rodinia plate reconstructions. Geology 31, 1053–1056.

Jefferson, C. W. and Parrish, R. R., 1989. Late Proterozoic stratigraphy, U-Pb zircon ages, and rift tectonics, Mackenzie Mountains, northwestern Canada. Canadian Journal of Earth Science 26,1784–1801.

Le Guerroué, E., Allen, P.A., Cozzi, A., Etienne, J.L., Fanning, M., 2006. 50 Myr recovery from the largest negative $\delta^{13}C$ excursion in the Ediacaran ocean. Terra Nova 18, 147–153.

MacLennan, S., Park, Y., Swanson-Hysell, N., Maloof, A., Schoene, B., Gebreslassie, M., Antilla, E., Tesema, T., Alene, M., Haileab, B., 2018. The arc of the Snowball: U-Pb dates constrain the Islay anomaly and the initiation of the Sturtian glaciation. Geology 46, 539–542.

McElreath, R., 2020. *Statistical Rethinking: A Bayesian Course with Examples in R and Stan, Second Edition*. Chapman and Hall/CRC (Boca Raton), 612 pp.

McKenzie, D., 1978. Some remarks on the development of sedimentary basins. *Earth and Planetary Science Letters* 40, 25–32.

Park, Y., Swanson-Hysell, N. L., MacLennan, S. A., Maloof, A. C., Gebreslassie, M., Tremblay, M. M., Schoene, B., Alene, M., Anttila, E. S. C., Tesema, T., and Haileab, B., 2020. The lead- up to the Sturtian Snowball Earth: Neoproterozoic chemostratigraphy time-calibrated by the Tambien Group of Ethiopia. Geological Society of America Bulletin 132, 1119–1149.

Rooney, A. D., Strauss, J. V., Brandon, A. D., and Macdonald, F. A., 2015. A Cryogenian chronology: Two long-lasting synchronous Neoproterozoic glaciations. Geology 43, 459–462.

Steckler, M.S. and Watts, A.B., 1978. Subsidence of the Atlantic-type continental margin off New York. *Earth and Planetary Science Letters* 41, 1–13.

Strauss, J. V., Macdonald, F. A., Halverson, G. P., Tosca, N. J., Schrag, D. P., and Knoll, A. H., 2015. Stratigraphic evolution of the Neoproterozoic Callison Lake Formation: Linking the break-up of Rodinia to the Islay carbon isotoep excursion. American Journal of Science 315, 881–944.

Strauss, J. V., Rooney, A. D., Macdonald, F. A., Brandon, A. D., Knoll, A. H., 2014. 740 Ma base-shaped microfossils from Yukon, Canada: Implications for Neoproterozoic chronology and biostratigraphy 740 Ma vase-shaped microfossils from Yukon, Canada: Implications for Neoproterozoic chronology and biostratigraphy. Geology 42, 659–662.

Swanson-Hysell, N. L., Maloof, A. C., Condon, D. J., Jenkin, G. R. T., Alene, M., Tremblay, M. M., Tesema, T., Rooney, A. D., and Haileab, B., 2015. Stratigraphy and geochronology of the Tambien Group, Ethiopia: Evidence for globally synchronous carbon isotope change in the Neoproterozoic. Geology 43, 323–326.

Vermeesch, P., 2018. IsoPlotR: A free and open toolbox for geochronology. Geoscience Frontiers 9, 1479–1493.

Section	Height (m)	Unit	d13C	d18O
G23	192.3	Ram Head Fm	3.66	-2.66
G23	188.6	Ram Head Fm	3.85	-4.07
G23	179.0	Ram Head Fm	2.80	-2.07
G23	174.0	Ram Head Fm	2.90	-1.35
G23	168.5	Ram Head Fm	3.37	-2.35
G23	162.2	Ram Head Fm	3.57	-3.68
G23	155.6	Ram Head Fm	4.92	-2.15
G23	149.5	Ram Head Fm	5.12	-2.01
G23	140.7	Ram Head Fm	2.75	-3.64
G23	134.6	Ram Head Fm	2.00	-2.49
G23	127.5	Ram Head Fm	2.81	-2.30
G23	121.0	Ram Head Fm	3.50	-3.63
G23	115.4	Ram Head Fm	4.62	-3.95
G23	106.0	Ram Head Fm	5.03	-3.83
G23	101.0	Ram Head Fm	3.15	-2.09
G23	94.7	Ram Head Fm	4.92	-3.59
G23	89.0	Ram Head Fm	4.01	-4.04
G23	84.0	Ram Head Fm	4.22	-2.81
G23	78.7	Ram Head Fm	4.10	-2.65
G23	73.6	Ram Head Fm	4.38	-0.54
G23	67.1	Ram Head Fm	5.70	-9.23
G23	61.8	Ram Head Fm	5.63	-8.81
G23	55.8	Ram Head Fm	6.77	-9.28
G23	49.8	Ram Head Fm	6.89	-9.98
G23	44.7	Ram Head Fm	4.18	-6.57
G23	40.0	Ram Head Fm	2.18	-8.55
G23	39.3	Ram Head Fm	2.93	-2.36
G23	23.7	Ram Head Fm	3.12	-3.07
G23	18.7	Ram Head Fm	4.02	-3.63
G23	13.9	Ram Head Fm	4.29	-3.61
G23	7.4	Ram Head Fm	6.40	-4.24
G23	0.0	Ram Head Fm	5.13	-4.51

height	mean d13C	95% max	95% min	median age	95% max	95% min
0	4.76	6.82	2.69	816.79	820.24	813.16
5	4.45	4.98	3.93	816.71	820.16	813.08
10	4.47	4.82	4.12	816.63	820.08	813
15	4.32	6.00	2.64	816.55	820	812.93
20	4.77	6.76	2.77	816.47	819.92	812.85
25	4.89	7.50	2.27	816.39	819.84	812.77
30	4.62	7.65	1.60	816.31	819.75	812.69
35	4.74	7.70	1.78	816.23	819.67	812.61
40	5.39	7.34	3.45	816.15	819.59	812.53
45	5.28	7.85	2.72	816.07	819.51	812.45
50	5.08	8.47	1.68	815.99	819.43	812.37
55	5.04	8.50	1.59	815.91	819.34	812.29
60	3.12	4.07	2.16	815.83	819.26	812.21
65	3.52	5.63	1.42	815.75	819.18	812.13
70	4.38	6.46	2.30	815.67	819.1	812.05
75	3.84	4.93	2.75	815.58	819.02	811.98
80	3.61	5.87	1.35	815.5	818.94	811.9
85	3.42	5.46	1.37	815.42	818.85	811.82
90	3.93	5.70	2.16	815.34	818.77	811.74
95	2.19	2.81	1.56	815.25	818.69	811.66
100	2.19	2.81	1.56	815.17	818.6	811.57
105	2.04	3.12	0.96	815.09	818.49	811.46
110	2.15	3.13	1.17	815.01	818.41	811.38
115	2.15	3.13	1.17	814.92	818.32	811.3
120	1.60	2.72	0.48	814.84	818.25	811.23
125	2.05	4.08	0.01	814.76	818.16	811.15
130	2.52	4.54	0.49	814.67	818.08	811.06
135	3.00	3.13	2.87	814.59	817.99	810.98
140	3.53	5.57	1.49	814.5	817.91	810.91
145	3.68	5.28	2.08	814.42	817.83	810.83
150	3.42	5.15	1.69	814.34	817.74	810.74
155	3.25	5.31	1.18	814.25	817.65	810.66
160	2.98	4.69	1.28	814.17	817.56	810.57
165	3.19	4.49	1.89	814.08	817.48	810.49
170	3.77	5.48	2.07	814	817.39	810.41
175	3.82	6.29	1.34	813.91	817.31	810.32
180	3.67	5.60	1.74	813.83	817.22	810.24
185	3.95	5.27	2.63	813.74	817.14	810.16
190	3.16	4.21	2.11	813.66	817.05	810.08
195	3.38	4.69	2.08	813.57	816.97	809.99
200	2.26	4.34	0.18	813.48	816.87	809.9
205	3.03	4.90	1.16	813.4	816.78	809.82
210	3.70	4.89	2.50	813.31	816.69	809.73
215	4.13	5.85	2.41	813.22	816.61	809.65
220	4.49	6.61	2.36	813.14	816.52	809.56
225	4.49	7.01	1.97	813.05	816.43	809.48
230	4.72	6.82	2.61	812.96	816.34	809.39
235	5.30	6.69	3.91	812.87	816.25	809.31
240	5.84	6.71	4.97	812.79	816.16	809.22
245	5.89	6.92	4.85	812.7	816.07	809.13
250	6.18	7.26	5.11	812.61	815.99	809.04
255	6.47	7.12	5.81	812.52	815.93	808.99
260	6.37	6.81	5.92	812.43	815.84	808.91
265	6.16	8.41	3.90	812.34	815.75	808.82
270	6.33	8.28	4.37	812.25	815.66	808.73
275	6.33	8.28	4.37	812.17	815.51	808.59
280	6.16	8.41	3.90	812.08	815.42	808.5
285	6.94	7.52	6.35	811.99	815.37	808.45
290	6.94	7.52	6.35	811.9	815.28	808.37
295	7.12	8.02	6.22	811.81	815.18	808.28
300	7.12	8.02	6.22	811.72	815.1	808.19
305	7.12	8.02	6.22	811.63	815	808.11
310	6.50	9.52	3.47	811.54	814.91	808.02
315	6.13	8.59	3.66	811.44	814.82	807.92
320	6.09	7.95	4.24	811.35	814.72	807.83
325	7.05	7.82	6.27	811.26	814.63	807.75
330	6.77	8.18	5.37	811.17	814.54	807.66
335	6.42	8.10	4.74	811.08	814.44	807.57
340	6.49	8.21	4.77	810.99	814.35	807.47
345	7.04	8.68	5.41	810.9	814.26	807.38
350	7.25	8.71	5.80	810.8	814.19	807.31
355	6.86	7.87	5.85	810.71	814.09	807.22
360	7.02	8.05	5.99	810.62	813.98	807.11
365	7.11	8.01	6.21	810.53	813.88	807.02
370	7.07	8.12	6.02	810.43	813.79	806.93
375	7.01	8.14	5.88	810.34	813.7	806.84
380	6.58	7.66	5.50	810.25	813.6	806.75
385	6.76	8.26	5.26	810.15	813.48	806.63
390	7.12	8.11	6.14	810.06	813.38	806.54
395	6.83	7.59	6.08	809.96	813.29	806.45
400	6.60	7.30	5.90	809.87	813.2	806.35
405	6.48	7.59	5.37	809.77	813.1	806.26
410	6.40	8.21	4.59	809.68	813	806.16
415	6.61	8.41	4.81	809.59	812.9	806.07
420	6.72	7.59	5.85	809.49	812.8	805.97
425	6.46	7.62	5.31	809.39	812.7	805.88

height	mean d13C	95% max	95% min	median age	95% max	95% min
430	6.59	7.95	5.23	809.3	812.68	805.85
435	6.73	7.88	5.57	809.2	812.58	805.76
440	6.46	7.54	5.39	809.1	812.48	805.66
445	5.75	8.65	2.86	809.01	812.38	805.57
450	4.99	9.08	0.90	808.91	812.2	805.39
455	3.81	9.00	-1.37	808.81	812.1	805.29
460	2.84	7.84	-2.15	808.71	812	805.2
465	1.35	6.19	-3.49	808.62	811.88	805.08
470	-0.70	0.48	-1.89	808.52	811.78	804.98
475	-0.90	0.03	-1.82	808.42	811.68	804.89
480	-0.93	-0.22	-1.63	808.32	811.58	804.79
485	-1.07	-0.48	-1.65	808.22	811.5	804.71
490	-1.10	-0.52	-1.68	808.12	811.37	804.59
495	-1.05	-0.21	-1.90	808.02	811.27	804.49
500	-1.17	-0.29	-2.05	807.92	811.11	804.33
505	-1.13	-0.11	-2.14	807.82	811	804.24
510	-0.93	0.20	-2.06	807.72	810.9	804.14
515	-1.02	-0.09	-1.95	807.62	810.79	804.04
520	-0.82	-0.01	-1.63	807.52	810.7	803.94
525	-0.68	-0.07	-1.29	807.42	810.59	803.84
530	-0.58	0.51	-1.67	807.32	810.49	803.74
535	-0.42	0.67	-1.52	807.22	810.39	803.64
540	-0.43	0.24	-1.10	807.12	810.27	803.53
545	-0.40	0.57	-1.36	807.02	810.16	803.42
550	-0.25	0.61	-1.11	806.92	810.06	803.32
555	-0.29	0.33	-0.91	806.81	809.98	803.24
560	-0.36	0.24	-0.96	806.71	809.89	803.16
565	-0.34	0.23	-0.91	806.61	809.79	803.06
570	-0.27	0.24	-0.77	806.5	809.68	802.97
575	-0.26	0.27	-0.79	806.4	809.58	802.87
580	-0.11	0.47	-0.70	806.3	809.47	802.77
585	-0.36	1.27	-1.99	806.19	809.37	802.67
590	-0.46	1.08	-2.00	806.09	809.26	802.57
595	-0.27	0.72	-1.27	805.98	809.16	802.47
600	-0.28	0.77	-1.33	805.88	809.05	802.36
605	-0.05	0.83	-0.92	805.77	808.94	802.26
610	-0.03	1.26	-1.33	805.67	808.83	802.15
615	-0.25	1.25	-1.75	805.56	808.73	802.05
620	-0.14	1.24	-1.53	805.46	808.57	801.9
625	0.07	1.90	-1.76	805.35	808.47	801.8
630	-0.21	1.75	-2.18	805.24	808.34	801.68
635	-0.35	1.28	-1.99	805.14	808.24	801.58
640	-0.65	1.43	-2.73	805.03	808.13	801.47
645	-0.96	1.08	-3.00	804.92	808.02	801.37
650	-0.74	0.99	-2.47	804.82	807.92	801.27
655	-0.62	1.26	-2.50	804.71	807.81	801.16
660	-0.87	1.16	-2.90	804.6	807.69	801.06
665	-0.73	0.81	-2.27	804.49	807.56	800.93
670	-1.03	0.06	-2.12	804.38	807.46	800.83
675	-1.23	-0.02	-2.44	804.27	807.35	800.73
680	-1.63	-0.12	-3.14	804.17	807.24	800.63
685	-1.81	-0.74	-2.88	804.06	807.13	800.52
690	-1.54	-0.46	-2.61	803.95	807.26	800.66
695	-1.70	-0.65	-2.76	803.84	807.15	800.56
700	-1.93	-0.36	-3.50	803.73	807.04	800.45
705	-1.79	-0.06	-3.52	803.61	806.92	800.34
710	-1.51	0.17	-3.20	803.5	806.81	800.23
715	-1.77	0.38	-3.91	803.39	806.7	800.12
720	-1.60	1.08	-4.27	803.28	806.59	800.01
725	-1.57	0.75	-3.89	803.17	806.48	799.91
730	-1.56	0.50	-3.61	803.06	806.37	799.8
735	-1.46	0.53	-3.45	802.94	806.25	799.69
740	-1.66	-0.43	-2.90	802.83	806.14	799.58
745	-1.94	-0.39	-3.49	802.72	806.03	799.47
750	-2.26	-0.63	-3.89	802.6	805.91	799.36
755	-2.23	-0.40	-4.06	802.49	805.79	799.25
760	-2.13	0.15	-4.40	802.37	805.68	799.14
765	-2.05	0.20	-4.30	802.26	805.56	799.02
770	-1.38	0.49	-3.25	802.14	805.44	798.91
775	-1.00	0.69	-2.69	802.03	805.27	798.74
780	-0.95	0.77	-2.67	801.91	805.16	798.63
785	0.94	3.86	-1.97	801.8	805.04	798.52
790	1.88	4.01	-0.26	801.68	804.92	798.41
795	2.43	3.95	0.90	801.56	804.8	798.29
800	2.84	4.49	1.18	801.45	804.67	798.17
805	3.13	4.76	1.50	801.33	804.55	798.06
810	3.35	4.64	2.07	801.21	804.43	797.95
815	3.53	5.66	1.40	801.09	804.31	797.83
820	3.52	5.51	1.54	800.97	804.19	797.71
825	3.68	5.02	2.34	800.86	804.07	797.59
830	3.81	5.13	2.48	800.74	803.89	797.42
835	5.06	7.14	2.97	800.62	803.77	797.31
840	5.25	6.76	3.74	800.5	803.65	797.19
845	5.21	6.81	3.61	800.38	803.54	797.08
850	5.62	6.99	4.25	800.25	803.41	796.96
855	5.87	7.76	3.99	800.13	803.29	796.84

height	mean d13C	95% max	95% min	median age	95% max	95% min
860	5.84	7.96	3.72	800.01	803.21	796.76
865	5.49	7.24	3.75	799.89	803	796.56
870	5.01	5.75	4.28	799.76	802.88	796.45
875	5.11	6.61	3.62	799.64	802.75	796.33
880	5.23	7.15	3.30	799.52	802.63	796.21
885	5.16	6.79	3.53	799.39	802.5	796.09
890	4.49	5.37	3.60	799.27	802.37	795.97
895	4.94	7.21	2.67	799.15	802.25	795.85
900	5.33	7.45	3.21	799.02	802.12	795.73
905	4.59	6.76	2.42	798.9	801.99	795.6
910	4.18	6.27	2.08	798.77	801.86	795.48
915	5.03	6.91	3.14	798.65	801.73	795.36
920	5.54	6.64	4.44	798.52	801.47	795.1
925	5.22	6.49	3.95	798.39	801.48	795.12
930	4.69	5.19	4.18	798.27	801.17	794.81
935	5.01	5.98	4.05	798.14	801.04	794.69
940	5.05	6.15	3.95	798.01	800.91	794.57
945	4.91	5.74	4.07	797.88	800.78	794.44
950	5.02	6.28	3.75	797.75	800.65	794.32
955	5.04	5.95	4.14	797.62	800.51	794.19
960	5.23	6.35	4.10	797.49	800.37	794.05
965	4.63	7.43	1.82	797.36	800.24	793.93
970	4.80	8.33	1.27	797.23	800.11	793.8
975	4.87	8.17	1.57	797.1	799.97	793.67
980	4.19	4.66	3.72	796.97	799.83	793.53
985	4.28	4.68	3.88	796.83	799.7	793.41
990	4.96	8.29	1.62	796.7	799.57	793.29
995	4.28	4.68	3.88	796.57	799.44	793.16
1000	3.78	4.64	2.92	796.44	799.28	793
1005	3.60	4.18	3.02	796.3	799.38	793.11
1010	4.17	5.16	3.17	796.17	799.24	792.98
1015	4.47	6.63	2.30	796.03	799.1	792.84
1020	4.44	6.15	2.73	795.9	798.97	792.71
1025	4.20	5.29	3.11	795.76	798.69	792.43
1030	4.18	5.12	3.24	795.62	798.54	792.3
1035	4.16	5.10	3.22	795.49	798.57	792.33
1040	4.39	6.20	2.57	795.35	798.17	791.93
1045	4.14	5.62	2.66	795.21	798.28	792.05
1050	5.03	5.80	4.25	795.07	797.89	791.67
1055	5.24	6.42	4.06	794.93	797.98	791.77
1060	5.59	6.35	4.83	794.79	797.84	791.63
1065	5.50	6.11	4.89	794.65	797.69	791.49
1070	5.30	6.16	4.44	794.51	797.55	791.35
1075	5.43	6.51	4.35	794.37	797.41	791.22
1080	5.73	6.07	5.38	794.23	797.27	791.08
1085	5.36	6.59	4.12	794.08	797.12	790.94
1090	5.30	6.88	3.73	793.94	796.98	790.81
1095	5.27	6.68	3.85	793.8	796.83	790.66
1100	5.02	6.71	3.33	793.66	796.69	790.53
1105	5.53	7.62	3.45	793.51	796.54	790.38
1110	5.54	6.94	4.14	793.37	796.4	790.25
1115	5.25	7.33	3.16	793.22	796.19	790.04
1120	4.90	7.04	2.75	793.08	796.04	789.9
1125	5.01	6.17	3.85	792.93	795.89	789.76
1130	5.38	6.95	3.81	792.78	795.74	789.62
1135	6.05	7.79	4.31	792.64	795.6	789.48
1140	6.11	7.13	5.09	792.49	795.45	789.34
1145	5.94	7.21	4.68	792.34	795.31	789.21
1150	6.09	6.87	5.31	792.19	795.17	789.08
1155	6.38	7.11	5.66	792.04	795.01	788.92
1160	6.72	7.66	5.78	791.89	794.85	788.77
1165	7.14	7.37	6.91	791.74	794.7	788.62
1170	7.04	7.55	6.53	791.59	794.53	788.47
1175	6.53	7.33	5.74	791.44	794.37	788.32
1180	6.23	7.32	5.14	791.28	794.22	788.16
1185	5.53	5.97	5.09	791.13	794.06	788.01
1190	5.50	5.86	5.13	790.98	793.9	787.86
1195	5.51	6.45	4.57	790.82	793.74	787.71
1200	5.49	6.39	4.58	790.67	793.58	787.56
1205	5.03	6.74	3.32	790.51	793.42	787.41
1210	4.77	6.41	3.12	790.36	793.32	787.31
1215	5.00	7.41	2.58	790.2	793.16	787.15
1220	5.00	7.41	2.58	790.04	792.96	786.97
1225	6.08	8.42	3.74	789.88	792.79	786.81
1230	6.81	8.20	5.42	789.72	792.63	786.66
1235	6.56	7.75	5.36	789.57	792.47	786.5
1240	7.11	7.76	6.45	789.41	792.3	786.34
1245	6.76	7.82	5.70	789.24	792.14	786.18
1250	6.44	7.61	5.27	789.08	791.98	786.02
1255	6.89	7.90	5.88	788.92	791.81	785.86
1260	6.55	7.78	5.32	788.75	791.64	785.7
1265	6.07	7.74	4.41	788.59	791.42	785.48
1270	6.35	7.65	5.04	788.43	791.24	785.31
1275	5.41	8.49	2.33	788.26	791.09	785.17
1280	6.28	9.18	3.37	788.1	790.88	784.97
1285	6.99	7.58	6.40	787.93	790.71	784.81

height	mean d13C	95% max	95% min	median age	95% max	95% min
1290	6.16	7.89	4.42	787.77	790.55	784.66
1295	6.16	7.89	4.42	787.6	790.38	784.49
1300	7.15	7.27	7.03	787.43	790.19	784.32
1305	7.13	7.69	6.57	787.26	790	784.12
1310	6.92	7.89	5.94	787.1	789.87	784
1315	6.49	7.75	5.23	786.93	789.68	783.82
1320	6.54	8.24	4.84	786.76	789.51	783.65
1325	6.64	8.18	5.10	786.59	789.34	783.49
1330	6.31	7.89	4.73	786.41	789.17	783.32
1335	6.53	8.26	4.80	786.24	788.99	783.15
1340	6.01	8.98	3.03	786.06	788.86	783.03
1345	5.53	8.31	2.75	785.89	788.68	782.86
1350	4.84	7.67	2.02	785.71	788.5	782.69
1355	4.84	7.67	2.02	785.53	788.33	782.53
1360	4.19	7.08	1.30	785.35	788.13	782.35
1365	4.18	7.07	1.28	785.18	787.95	782.17
1370	4.81	6.30	3.32	785	787.77	781.99
1375	4.37	7.34	1.39	784.81	787.58	781.81
1380	4.25	6.24	2.27	784.63	787.41	781.65
1385	4.16	5.88	2.45	784.45	787.22	781.46
1390	3.75	5.07	2.44	784.27	787.04	781.28
1395	3.43	4.17	2.68	784.09	786.86	781.11
1400	3.91	6.78	1.03	783.9	786.67	780.93
1405	4.17	6.63	1.71	783.71	786.44	780.71
1410	4.11	5.94	2.28	783.53	786.25	780.54
1415	3.41	5.89	0.93	783.34	786.07	780.35
1420	3.82	7.17	0.47	783.15	785.87	780.16
1425	5.57	8.24	2.91	782.97	785.67	779.98
1430	5.52	7.56	3.49	782.78	785.48	779.79
1435	4.89	6.15	3.62	782.59	785.28	779.6
1440	5.01	6.43	3.60	782.39	785.08	779.41
1445	5.58	7.65	3.52	782.2	784.89	779.22
1450	6.02	8.00	4.05	782.01	784.7	779.03
1455	6.59	8.86	4.32	781.81	784.49	778.84
1460	7.53	10.58	4.48	781.62	784.29	778.64
1465	7.59	9.89	5.29	781.42	784.08	778.45
1470	7.43	9.00	5.86	781.22	783.88	778.25
1475	7.52	9.35	5.69	781.02	783.68	778.06
1480	7.51	9.33	5.69	780.82	783.49	777.87
1485	7.70	8.75	6.65	780.62	783.29	777.67
1490	6.97	9.34	4.60	780.42	783.11	777.5
1495	6.69	9.07	4.32	780.22	782.92	777.32
1500	7.15	8.13	6.16	780.01	782.7	777.11
1505	7.28	7.91	6.66	779.81	782.5	776.91
1510	7.33	8.24	6.41	779.6	782.29	776.71
1515	6.94	9.00	4.89	779.39	782.11	776.54
1520	6.70	9.01	4.39	779.18	781.9	776.34
1525	7.81	8.98	6.64	778.98	781.71	776.15
1530	7.67	8.91	6.42	778.77	781.45	775.9
1535	7.47	8.36	6.58	778.56	781.29	775.74
1540	7.58	8.30	6.86	778.35	781.09	775.54
1545	7.86	8.80	6.93	778.14	780.83	775.29
1550	7.83	9.16	6.50	777.92	780.6	775.06
1555	7.57	8.81	6.32	777.71	780.42	774.89
1560	7.46	9.13	5.79	777.49	780.21	774.69
1565	7.48	9.52	5.45	777.27	779.98	774.46
1570	7.83	8.85	6.82	777.05	779.75	774.24
1575	7.68	9.48	5.87	776.83	779.53	774.02
1580	7.63	9.51	5.75	776.61	779.31	773.79
1585	7.77	9.06	6.48	776.38	779.02	773.51
1590	7.99	9.05	6.92	776.16	778.8	773.29
1595	7.52	9.24	5.81	775.93	778.66	773.16
1600	6.65	8.72	4.57	775.71	778.43	772.94
1605	5.94	8.90	2.98	775.48	778.26	772.78
1610	5.78	9.07	2.50	775.24	778.03	772.55
1615	5.86	8.72	2.99	775.01	777.74	772.26
1620	5.44	6.54	4.34	774.78	777.52	772.04
1625	5.15	6.30	3.99	774.54	777.28	771.81
1630	5.10	6.40	3.79	774.31	777.04	771.58
1635	6.41	9.60	3.22	774.07	776.82	771.35
1640	7.01	9.55	4.46	773.83	776.58	771.11
1645	5.87	9.23	2.51	773.59	776.36	770.9
1650	5.06	9.80	0.32	773.35	776.12	770.66
1655	4.89	8.61	1.17	773.11	775.89	770.43
1660	5.36	9.40	1.31	772.86	775.65	770.19
1665	4.43	9.28	-0.41	772.61	775.4	769.94
1670	3.23	7.30	-0.85	772.36	774.88	769.42
1675	3.86	8.60	-0.89	772.12	774.87	769.42
1680	5.41	8.40	2.42	771.86	774.39	768.94
1685	4.78	9.12	0.43	771.61	774.13	768.69
1690	5.20	6.98	3.41	771.36	774.07	768.62
1695	5.73	7.73	3.74	771.1	773.72	768.28
1700	5.40	6.58	4.22	770.84	773.46	768.02
1705	6.57	8.21	4.93	770.58	773.2	767.75
1710	6.59	8.01	5.17	770.31	772.85	767.41
1715	7.00	7.69	6.32	770.05	772.59	767.15

height	mean d13C	95% max	95% min	median age	95% max	95% min
1720	7.09	7.75	6.42	769.79	772.33	766.89
1725	7.05	7.64	6.46	769.52	772.07	766.62
1730	7.12	7.86	6.39	769.26	771.81	766.35
1735	7.15	7.91	6.39	768.98	771.63	766.17
1740	7.13	8.95	5.30	768.71	771.57	766.1
1745	6.40	9.24	3.56	768.44	771.25	765.79
1750	6.89	9.65	4.12	768.16	770.98	765.51
1755	6.81	9.27	4.36	767.89	770.71	765.23
1760	6.49	8.21	4.77	767.6	770.39	764.9
1765	7.35	8.99	5.71	767.32	770.1	764.61
1770	6.73	8.29	5.16	767.04	769.83	764.33
1775	7.81	8.33	7.28	766.75	769.5	764
1780	7.69	8.38	7.00	766.46	769.07	763.56
1785	7.81	8.33	7.28	766.17	768.76	763.25
1790	7.59	8.74	6.43	765.88	768.58	763.06
1795	7.80	8.57	7.03	765.59	768.21	762.69
1800	7.93	9.14	6.73	765.3	767.92	762.39
1805	8.05	9.24	6.85	764.99	767.64	762.11
1810	7.97	9.78	6.16	764.69	767.35	761.8
1815	8.06	9.88	6.23	764.39	767.06	761.5
1820	8.46	9.58	7.33	764.08	766.77	761.2
1825	8.40	9.98	6.82	763.77	766.48	760.9
1830	8.18	9.32	7.05	763.46	766.18	760.58
1835	8.54	9.95	7.14	763.14	765.88	760.27
1840	7.92	10.43	5.41	762.82	765.59	759.96
1845	8.13	9.91	6.35	762.5	765.29	759.63
1850	8.58	9.43	7.74	762.18	765	759.33
1855	8.33	9.90	6.76	761.85	764.68	758.99
1860	8.21	9.64	6.78	761.53	764.38	758.65
1865	8.35	9.49	7.20	761.2	764.07	758.3
1870	8.22	9.48	6.96	760.86	763.76	757.96
1875	7.90	9.32	6.47	760.53	763.45	757.61
1880	7.55	10.08	5.01	760.19	763.16	757.28
1885	7.46	10.16	4.77	759.85	762.8	756.89
1890	7.21	9.91	4.51	759.51	762.49	756.54
1895	6.37	9.87	2.87	759.16	762.13	756.15
1900	5.76	10.16	1.37	758.81	761.84	755.81
1905	5.74	10.48	1.00	758.46	761.51	755.44
1910	6.96	7.75	6.17	758.1	761.12	755.01
1915	7.03	7.91	6.16	757.74	760.79	754.64
1920	7.03	7.75	6.32	757.38	760.27	754.09
1925	6.14	8.45	3.84	757.01	759.87	753.65
1930	5.57	8.09	3.05	756.64	759.51	753.25
1935	4.50	6.94	2.06	756.26	759.14	752.84
1940	4.34	6.67	2.02	755.89	758.8	752.43
1945	4.50	6.33	2.68	755.5	758.43	752.01
1950	4.33	5.94	2.72	755.12	758.08	751.6
1955	4.27	5.81	2.73	754.74	757.74	751.19
1960	4.49	6.03	2.95	754.35	757.38	750.76
1965	4.15	6.89	1.41	753.95	757.17	750.48
1970	4.11	7.66	0.57	753.55	756.61	749.86
1975	4.96	8.27	1.65	753.15	756.23	749.42
1980	5.16	8.09	2.24	752.75	755.84	748.95
1985	5.21	7.81	2.60	752.34	755.51	748.56
1990	5.27	8.34	2.20	751.92	755.1	748.07
1995	5.46	8.66	2.26	751.5	754.7	747.6
2000	6.09	8.86	3.32	751.08	754.45	747.26
2005	6.50	8.73	4.28	750.64	754.02	746.75
2010	6.42	8.14	4.71	750.21	753.58	746.23
2015	6.37	8.14	4.61	749.77	753.17	745.72
2020	6.98	7.60	6.36	749.31	753.01	745.47
2025	7.03	7.59	6.48	748.86	752.56	744.95
2030	5.52	11.09	-0.05	748.4	751.9	744.19
2035	4.50	9.35	-0.34	747.95	751.75	743.94
2040	3.67	6.10	1.24	747.48	751.27	743.36
2045	3.69	5.77	1.61	747.01	750.9	742.9
2050	3.25	6.24	0.25	746.53	750.45	742.34
2055	3.44	7.18	-0.30	746.05	750.04	741.81
2060	3.64	6.78	0.49	745.56	749.6	741.24
2065	2.47	5.06	-0.12	745.07	749.17	740.69
2070	1.97	4.74	-0.80	744.56	748.73	740.12
2075	1.64	4.23	-0.94	744.06	748.06	739.32
2080	2.43	5.30	-0.45	743.54	747.85	738.97
2085	3.11	7.86	-1.63	743.01	747.38	738.36
2090	2.21	9.55	-5.13	742.47	746.88	737.7
2095	-0.51	7.44	-8.46	741.93	746.29	736.97
2100	-0.25	6.48	-6.97	741.38	745.76	736.29
2105	-0.62	4.48	-5.72	740.83	745.42	735.8
2110	-1.37	2.31	-5.05	740.27	744.91	735.12
2115	-1.54	0.28	-3.36	739.7	744.44	734.46
2120	-3.04	-0.84	-5.24	739.12	743.91	733.74
2125	-4.44	-2.66	-6.21	738.55	743.44	733.05
2130	-5.05	-3.32	-6.79	737.94	742.94	732.35

Sample nam	Unit	Reference section height (m)	Median Age (Myr)	Age upper bound	Age lower bound	$\delta^{13}C_{carb}$ (‰)	$\delta^{18}O_{carb}$ (‰)	$^{87}Sr/^{86}Sr$	Sr (ppm)	Mn/Sr	Reference
G332-489.9	Russøya Mb.	2105.3	740.79	745.4	735.76	-4.0	-5.0	0.70675			Halverson et al. (2007)
G22-9.1	Russøya Mb.	2050.2	746.51	750.43	742.31	0.9	-4.1	0.70674	623	0.07	Halverson et al. (2007)
G22-1.3	Russøya Mb.	2042.4	747.26	751.07	743.12			0.70672	542	0.06	Halverson et al. (2007)
G332-377.6	Russøya Mb.	2022	749.13	752.83	745.27	7.1	-4.1	0.70675			Halverson et al. (2007)
G523-31.4	Russøya Mb.	1987.1	752.16	755.34	748.35	4.4	-4.6	0.70679	354		Cox et al. (2016)
G523-29.3	Russøya Mb.	1985	752.34	755.51	748.56	4.0	-3.7	0.70662	1290		Cox et al. (2016)
G523-27	Russøya Mb.	1982.7	752.53	755.68	748.77	3.6	-3.9	0.70700	1120		Cox et al. (2016)
G523-24.8	Russøya Mb.	1980.5	752.71	755.83	748.94	3.0	-4.3	0.70668	990		Cox et al. (2016)
G523-23.3	Russøya Mb.	1979	752.83	755.93	749.06	2.7	-5.2	0.70701	899		Cox et al. (2016)
G523-22.4	Russøya Mb.	1978.1	752.9	756	749.15	2.6	-5.0	0.70669	1360		Cox et al. (2016)
G4-49.1	Russøya Mb.	1970.1	753.55	756.6	749.85	2.7	-6.4	0.70677	358	0.16	Halverson et al. (2007)
M6-131.8	Backlund. Fm.	1571.4	776.99	779.69	774.18	8.2	-4.9	0.70687	1860	0.00	Halverson et al. (2007)
M6-102.9	Backlund. Fm.	1542.5	778.24	780.94	775.4	8.0	-5.9	0.70690	2740	0.01	Halverson et al. (2007)
G15-90.1	Backlund. Fm.	1534.7	778.57	781.31	775.76	7.2	-5.9	0.70693	2560	0.02	Halverson et al. (2007)
G15-78.6	Backlund. Fm.	1523.2	779.05	781.78	776.22	7.5	-5.8	0.70695	2980	0.01	Halverson et al. (2007)
G15-45.6	Backlund. Fm.	1490.2	780.41	783.1	777.5	7.9	-5.3	0.70697	2540	0.00	Halverson et al. (2007)
G15-29.8	Backlund. Fm.	1474.4	781.05	783.71	778.09	8.2	-6.1	0.70697	3380	0.01	Halverson et al. (2007)
G35-25.8	Svanberg. Fm.	921	798.5	801.42	795.05	4.9	-7.5	0.70649	739	0.02	Halverson et al. (2007)
G35-0.3	Svanberg. Fm.	895.5	799.07	802.17	795.77	5.2	-8.3	0.70634	942	0.01	Halverson et al. (2007)
G341-445.3	Svanberg. Fm.	898.1	799.14	802.23	795.84	4.3	-6.1	0.70661	1030	0.03	Halverson et al. (2007)
G37-53.0	Svanberg. Fm.	846.2	800.21	803.36	796.91	6.2	-6.7	0.70617	1890	0.01	Halverson et al. (2007)
G37-28.8	Svanberg. Fm.	822	800.35	803.51	797.05	4.1	-6.5	0.70651	739	0.10	Halverson et al. (2007)
G19-71.8	Svanberg. Fm.	852	800.56	803.72	797.25	6.0	-6.3	0.70625	993	0.07	Halverson et al. (2007)
G19-57.2	Svanberg. Fm.	837.4	800.93	804.14	797.66	5.9	-6.8	0.70629	964	0.06	Halverson et al. (2007)
G37-27.8	Svanberg. Fm.	821	800.95	804.16	797.69			0.70644	780	0.09	Halverson et al. (2007)
G155-130	Svanbergfjelle	761	802.35	805.65	799.11	-2.45	-5.91	0.70636	651	0.05	Halverson et al. (2007)
G155-124.6	Svanbergfjelle	755.6	802.47	805.78	799.24	0.13	-6.42	0.70639	1040	0.01	Halverson et al. (2007)
G341-282.5	Svanberg. Fm.	735.3	802.94	806.25	799.68	0.0	-5.5	0.70635	536	0.07	Halverson et al. (2007)
G155-96.1	Svanbergfjelle	727.1	803.12	806.43	799.86	-1.68	-6.66	0.70646	753	0.02	Halverson et al. (2007)
G155-88.2	Svanbergfjelle	719.2	803.3	806.61	800.03	-0.92	-6.44	0.70646	584	0.02	Halverson et al. (2007)
G341-215.6	Svanberg. Fm.	668.4	804.42	807.5	800.87	-0.7	-6.9	0.70634	930	0.02	Halverson et al. (2007)
G341-205.1	Grusdiev. Fm.	657.9	804.65	807.74	801.1	-2.1	-7.3	0.70644	368	0.08	Halverson et al. (2007)
G341-178	Grusdiev. Fm.	630.8	805.23	808.33	801.66	-0.3	-7.3	0.70642	806	0.02	Halverson et al. (2007)
M9-125.6	Grusdiev. Fm.	621.4	805.43	808.54	801.87	0.6	-8.5	0.70660	1240	0.00	Halverson et al. (2007)
G341-146.6	Grusdiev. Fm.	599.4	805.89	809.06	802.37	0.1	-6.9	0.70637	1480	0.01	Halverson et al. (2007)
M9-83.4	Grusdiev. Fm.	579.2	806.31	809.49	802.78	-0.3	-8.5	0.70641	2030	0.00	Halverson et al. (2007)
M9-55	Grusdiev. Fm.	550.8	806.9	810.05	803.31	-0.7	-9.2	0.70640	2280	0.00	Halverson et al. (2007)
G33-145.9	Grusdiev. Fm.	498.2	807.96	811.14	804.37	-1.1	-8.3	0.70643	1240	0.00	Halverson et al. (2007)
G33-131.7	Grusdiev. Fm.	483.9	808.24	811.52	804.73	-1.2	-8.5	0.70644	594	0.02	Halverson et al. (2007)
G148-158.7	Grusdiev. Fm.	476.8	808.38	811.57	804.78	-1.2	-8.1	0.70635	696	0.02	Halverson et al. (2007)
G148-136.3	Grusdiev. Fm.	454.4	808.82	812.11	805.3	0.3	-8.8	0.70624	282	0.10	Halverson et al. (2007)
G148-126	Grusdiev. Fm.	444.1	809.02	812.4	805.59	6.4	-7.0	0.70625	1720	0.01	Halverson et al. (2007)
G33-91	Grusdiev. Fm.	443.2	809.04	812.42	805.6	5.8	-10.6	0.70652	514	0.01	Halverson et al. (2007)
G33-62.2	Grusdiev. Fm.	414.2	809.6	812.91	806.08	7.3	-7.1	0.70628	1690	0.00	Halverson et al. (2007)
G33-14.5	Grusdiev. Fm.	366.7	810.5	813.85	806.99	6.6	-6.3	0.70626	2530	0.00	Halverson et al. (2007)
G336-281.7	Grusdiev. Fm.	281.7	812.05	815.39	808.47	7.0	-5.7	0.70627	2280	0.01	Halverson et al. (2007)